Effect of Concrete/CFRP Interface Modeling on Failure Assessment of RC Beams Strengthened with CFRP Plates: A Cohesive Element Model

Thanawat Treetrisit[a], Suchart Limkatanyu[b] and Kittisak Kuntiyawichai[c,*]

[a]Postgraduate student, Department of Civil Engineering, Ubonratchathani University, Ubonratchathani 34190, Thailand.
[b]Department of Civil Engineering, Prince of Songkla University, Songkla 90000, Thailand.
[c]Department of Civil Engineering, Ubonratchathani University, Ubonratchathani 34190, Thailand.
[*]Corresponding author. E-mail address: kittisak.ubu@gmail.com (K. Kuntiyawichai)

Received 26 January 2009; accepted 15 December 2009

Abstract

The present paper investigates the effect of concrete/CFRP interface modeling on failure assessment of RC beams strengthened with CFRP plates using finite element technique (FE). From the previous studies, it was found that most of the FE studies neglected the interaction between concrete/CFRP interface by either assuming perfectly bond or using simple solid element between the interfaces. This can affect the accuracy of the results obtained from FE model especially the failure pattern of RC beams strengthened with CFRP plates. Therefore, in order to capture the real behavior of concrete/CFRP interface which influences the prediction of failure pattern of the beams, cohesive elements, which have the ability on modeling adhesives and bonded interfaces, are used to model traction and shear behavior of concrete/CFRP interface. Ten case studies with various parameters, i.e. thickness of FRP plates, length of FRP plates and types of reinforcement, are chosen from the literatures to perform analysis using ABAQUS. The results obtained from FE models show good agreement with the experimental data in terms of loading capacity, failure pattern, shear stresses distribution at concrete/CFRP interface and strains distribution in CFRP plates. It is evident that the discontinuities of the shear stresses distribution along concrete/CFRP interface are actually associated with the location of cracks occurring at concrete beams whereas the progressive de-cohesion of the laminate from the concrete face initiating in the area near to the point of high shear stresses. In addition, cracks location can be obtained with close agreement with experimental data.

Keywords: Cohesive element; Shear stresses distribution; RC beam; CFRP plates; Finite element modeling

INTRODUCTION

Since 1990, application of Carbon Fiber Reinforced Polymer (CFRP) in strengthening of reinforced concrete (RC) structures has become an attractive retrofit manner. The main advantages of CFRP in general for CFRP strips are their high strength/weight and stiffness/weight ratios, high degree of chemical inertness in most civil engineering environments, and their non-magnetic and non-conductive properties (Mayo et al., 2000). CFRP materials have mechanical and physical properties superior to those of steel, especially with respect to tensile and fatigue strengths. Furthermore, no heavy mechanized lifting equipments and clamping devices are needed due to their lightweights and consequently the costs of application are reduced.

To study the behavior of reinforced concrete structures strengthened by CFRP, it is essential to understand the effects of repair on the failure mode of the strengthened member. It has been observed that different failure mechanisms ranging from ductile to very brittle occur as externally bonded reinforcement is added to a flexural member. A number of failure modes for RC beams bonded with FRP sheets or strips have been observed in numerous experimental investigations (Arduini & Nanni, 1997; Triantafillou & Plevris, 1992). The failure modes can be classified into seven main categories: *(a)* flexural failure by FRP rupture; *(b)* flexural failure by crushing of compressive concrete; *(c)* shear failure; *(d)* concrete cover separation; *(e)* plate-end shear debonding; *(f)* intermediate flexural crack-induced debonding; *(g)* intermediate flexural shear crack-induced debonding. However most common failure modes found in the experimental results are debonding of the CFRP plate and concrete cover separation. These failure modes lead to premature failure of the beam occurring before the ultimate flexural capacity. It is generally believed that these failure modes are initiated by the formation of a crack at or near the plate ends due to high shear and normal stresses caused by the abrupt termination of the plate. Once a crack forms in the concrete at or near the plate ends, the crack propagates to the level of the tension reinforcement and then progresses horizontally along the level of the internal steel reinforcement, resulting in the separation of the concrete cover.

Although experimental investigations are essential in understanding the behavior of the premature failure of the beam under concrete cover separation, analytical and numerical studies are also needed in order to further comprehend and predict these failure modes. For analytical studies, the close-form solutions for determine the shear stresses have also been proposed for the last decade (Robert, 1989; Malek et al., 1998; Smith & Teng, 2001). However, these existing solutions were based on specific assumptions

and limitations. For numerical studies, several researchers (Ziraba & Baluch, 1995; Arduini et al., 1997; Wong et al., 2003) conducted a finite element analysis of CFRP strengthened beams under different approaches and found that finite element results were able to predict the experimental results such as load-deflection behavior and non-linear behavior of concrete. However, it was found that most of the FE studies neglected the interaction between concrete/CFRP interface by either assuming perfectly bond or using simple solid element between the interfaces. This can affect the accuracy of the results obtained from FE model. Therefore, in order to capture the real behavior between two surfaces, care should be taken when modeling concrete/CFRP interface.

In this study, cohesive elements which able to capture damage initiation due to shear stress are used to model traction and shear behavior of concrete/CFRP interface. Ten case studies with various parameters, i.e. thickness of FRP plates, length of FRP plates and types of reinforcement, are chosen from the literatures to perform analysis using ABAQUS (Hibbitt et al., 2005). The results of the study are presented and discussed in terms of shear stress distribution between concrete/CFRP interface, loading capacity, failure pattern and strains distribution and CFRP plates.

MATERIALS AND METHODS

Experimental data

Experimental data were obtained from Rahimi and Hutchinson (Rahimi & Hutchinson, 2001) and Fanning and Kelly (Fanning & Kelly, 2001). A total of 10 beams, strengthened with CFRP were selected for comparison with the numerical results. The failure modes for selected beams were cover failure and concrete crushing. The details of each experimental study are summarized below;

Rahimi and Hutchinson's experiment

Figure 1 shows geometric properties and test arrangement of Rahimi and Hutchinson experiment. Two series (B and C) of test specimens were chosen which comprise the internal and external reinforcements summarized in Tables 1 and 2. The beams RH-B1 and RH-C1 are control beams whereas the rests are strengthened with different thicknesses of CFRP. Material properties are summarized in Table 3.

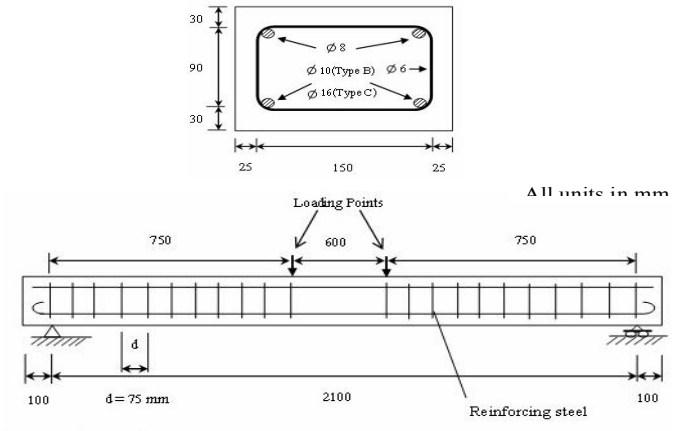

Figure 1. Geometric properties and test arrangement (Rahimi & Hutchinson, 2001).

Table 1. Details of internal reinforcements of test beams (Rahimi & Hutchinson, 2001)

Beam type	Conventional Reinforcements			External reinforcement [a]
	Tensile	Compressive	Shear	
B	2T10 (A_s/bd=0.65%)	2T8 (A_s/bd=0.42%)	R6 links at 75-mm centers	CFRP plates (0.4 and 1.2 mm)
C	2T16 (A_s/bd=1.68%)	2T8 (A_s/bd=0.42%)	R6 links at 75-mm centers	CFRP plates (0.4 and 1.2 mm)

Note: Shear links were placed only within shear spans of beams.

[a] Plate thickness.

Table 2. Details of External Reinforcements of Test Beams (Rahimi & Hutchinson, 2001)

Beam Nomenclatures	Type of external reinforcement and plate thickness	Beam width (mm)	Beam depth (mm)	Beam length (mm)	CFRP length (mm)	CFRP width (mm)	CFRP thickness (mm)
RH-B1	None	200	150	2300	-	-	-
RH-B3	CFRP laminate, 2 ply (0.4 mm)	200	150	2300	1930	150	0.4
RH-B5	CFRP laminate, 6 ply (1.2 mm)	200	150	2300	1930	150	1.2
RH-C1	None	200	150	2300	-	-	-
RH-C3	CFRP laminate, 2 ply (0.4 mm)	200	150	2300	1930	150	0.4
RH-C5	CFRP laminate, 6 ply (1.2 mm)	200	150	2300	1930	150	1.2

Table 3. Material properties for test beams (Rahimi & Hutchinson, 2001)

Property (20◦C)	Concrete	CFRP composite	Sikadur 31 PBA adhesive	Internal steel reinforcement
Density (kg/m^3)	200	1,500	1,500	7,800
Young's modulus (GN/m^2)	25	127	7	210
Shear strength (MN/m^2)	6	80[a]	27	-
Tensile strength (MN/m^2)	3	1532	25	575
Compressive strength(MN/m^2)	54-69	-	70	-
Fracture energy (kJ/m^2)	0.02	-	0.4	-
Poisson's ratio	0.2	0.3	0.3	0.3
Elongation at break (%)	0.15	1.21	0.7	>20
Coefficient of thermal expansion(10^{-6}/C)	10	-0.8	30	11

Note: GFRP and CFRP properties quoted in fiber direction

[a] Interlaminar shear strength

Fanning and Kelly's Experiment

Figure 2 shows internal reinforcements, geometric properties and test arrangement of Fanning and Kelly experiment. The external reinforcements are summarized in Table 4. The beam FK-B1 is the control beam whereas the rests are strengthened with different CFRP lengths. Material properties are summarized in Table 5.

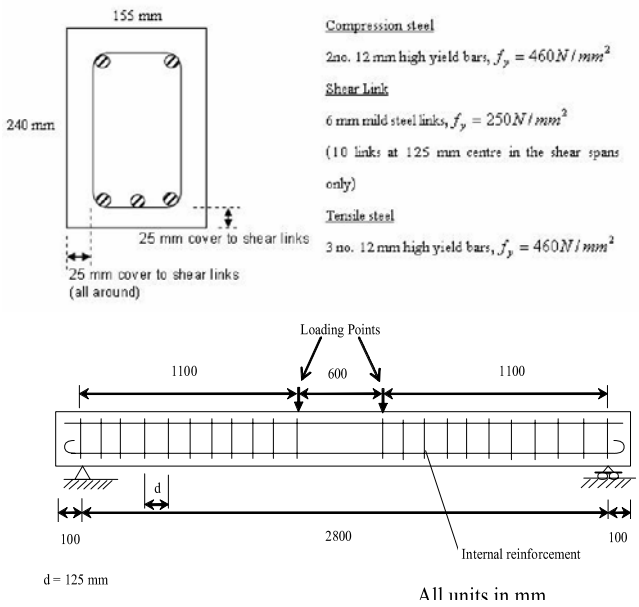

Figure 2. Geometric properties and test arrangement (Fanning & Kelly, 2001).

Table 4. Details of external reinforcements of test beams (Fanning & Kelly, 2001)

Beam Nomenclatures	Type of external reinforcement and plate thickness	Beam width (mm)	Beam depth (mm)	Beam length (mm)	FRP length (mm)	FRP width (mm)	FRP thickness (mm)
FK-B1	None	155	240	3000	-	-	-
FK-B3	CFRP laminate	155	240	3000	3000	120	1.2
FK-B5	CFRP laminate	155	240	3000	2030	120	1.2
FK-B9	CFRP laminate	155	240	3000	1700	120	1.2

Table 5. Material properties for test beams (Fanning & Kelly, 2001)

Material Properties	Concrete	High yield steel	Mild steel	Adhesive	CFRP composite material plates
Elastic moduli (GPa)	39.2	210	210	11.6	155(Long) 10(Trans)
Poisson's ratio	0.27	0.3	0.3	0.3	0.3(Major) 0.0194(Minor)
Tensile strength (MPa)	5	460	250	45	1532
Compressive strength (MPa)	80	NA	NA	NS	NA
Shear transfer coefficient	1.0	NA	NA	1.0	NA
Yield strength (MPa)	NA	460	250	NA	NA
Post-yield stiffness (GPa)	NA	0	0	NA	NA

NA: not applicable; NS: not specified

Material constitutive models

This section presents material constitutive models including concrete model, steel model adhesive model and CFRP. The details of each constitutive model are summarized below;

Concrete model

The concrete model used in this study is a continuum, plasticity-based, damage model (Bazant, 1986; Lubliner et al., 1989). It assumes that the main two failure mechanisms are tensile cracking and compressive crushing of the concrete material. The evolution of the yield surface is controlled by two hardening variables, i.e. tensile and compressive equivalent plastic strains, linked to failure mechanisms under tension and compression loading, respectively.

Uniaxial Tension Behavior

The model assumes that the uniaxial tensile response of concrete is characterized by damaged plasticity, as shown in Figure 3. Under uniaxial tension the stress-strain response follows a linear elastic relationship until the value of the failure stress isreached. The failure stress corresponds to the onset of micro-cracking in the concrete material. Beyond the failure stress the formation of micro-cracks is represented macroscopically with a softening stress-strain response, which induces strain localization in the concrete structure. Equation 1 presents the stress-strain relations of concrete under uniaxial tension.

$$\sigma_t = (1 - d_t) E_0 \left(\varepsilon_t - \tilde{\varepsilon}_t^{pl}\right) \qquad (1)$$

where σ_t is tensile stress, d_t is damage variable which is assumed to be a function of tensile plastic strains ($\tilde{\varepsilon}_t^{pl}$), E_0 is modulus of elasticity of concrete and ε_t is tensile strains.

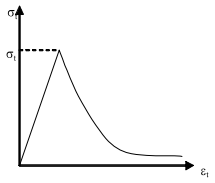

Figure 3. Response of concrete to uniaxial loading in tension (Hibbitt et al., 2005).

Uniaxial Compression Behavior

Under uniaxial compression the response is linear until the value of initial yield (σ_{c0}) In the plastic regime the response is typically characterized by stress hardening followed by strain softening beyond the ultimate stress, (σ_{cu}) as shown in Figure 4.

Equation 2 presents the stress-strain relations of concrete under uniaxial tension.

$$\sigma_c = (1 - d_c) E_0 \left(\varepsilon_c - \tilde{\varepsilon}_c^{pl}\right) \quad (2)$$

where σ_c is compressive stress, d_c is damage variable

which is assumed to be a function of compressive plastic strains ($\tilde{\varepsilon}_c^{pl}$), E_0 is modulus of elasticity of concrete and ε_t is compressive strains.

Steel model

The stress-strain curve for steel reinforcement is assumed to be elastic perfectly plastic. This means that steel reinforcement behaves elastically up to the yield point. After that the yield stress does not change with plastic strain. This can be seen in Figure 5.

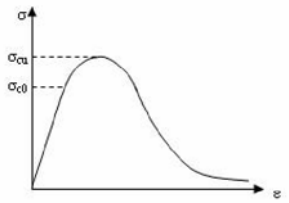

Figure 4. Response of concrete to uniaxial loading in compression (Hibbitt et al., 2005).

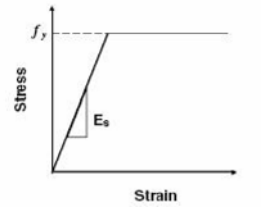

Figure 5. Elastic perfectly plastic model for steel reinforcement.

Adhesive model

The adhesive behavior is monitored using cohesive elements which are useful in modeling adhesives and bonded interfaces. The cohesive elements model the initial loading, the initiation of damage, and the propagation of damage leading to eventual failure at the bonded interface. The behavior of the interface prior to initiation of damage is often described as linear elastic in terms of a penalty stiffness that degrades under tensile and/or shear loading but is unaffected by pure compression (see Figure 6). Damage is assumed to initiate when a quadratic interaction function involving the nominal stress ratios (as defined in the expression below) reaches a value of one. This criterion can be represented as;

$$\left\{\frac{t_n}{t_n^o}\right\}^2 + \left\{\frac{t_s}{t_s^o}\right\}^2 + \left\{\frac{t_t}{t_t^o}\right\}^2 = 1 \qquad (3)$$

where t_n, t_s and t_t represent the nominal stress when the deformation is either purely normal to the interface or purely in the first or the second shear direction, respectively t_n^o, t_s^o and t_t^o represent the peak values of the nominal stress when the deformation is either purely normal to the interface or purely in the first or the second shear direction, respectively.

The rate at which the material stiffness is degraded once the corresponding initiation criterion is reached can be described by the damage evolution law as shown in equation 4.

$$\begin{aligned} t_n &= (1-D)\bar{t}_n, \quad \bar{t}_n \geq 0 \\ t_s &= (1-D)\bar{t}_s \\ t_t &= (1-D)\bar{t}_t \end{aligned} \qquad (4)$$

where a scalar damage variable, D, represents the overall damage in the material and captures the combined effects of all the active mechanisms $\bar{t}_n, \bar{t}_s$ and $\bar{t}_t$ are the stress components predicted by the elastic traction-separation behavior for the current strains without damage.

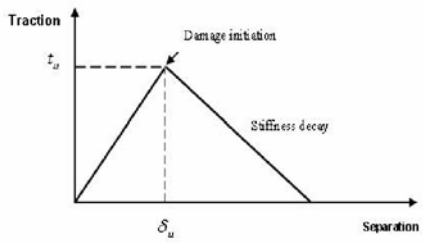

Figure 6. Linear elastic traction separation behavior of cohesive element.

CFRP model

The brittle cracking model is employed in CFRP modeling. The stress-strain behavior of CFRP is assumed to be elastic up to failure strain. At this stage, a crack develops and the material loses all its load-carrying capacity (see Figure 7).

Finite element model

The input data for the finite element models was generated by using the general purpose pre and post processing code PATRAN (PDA Engineering, 1993). The complete model was then analyzed by the ABAQUS finite element package. Two dimensional solid elements with four nodes, i.e. CPE4R, were used for modeling concrete materials.

For steel reinforcement,two dimensional truss elements, i.e. T2D2, were used. In order to enhance the accuracy of the model, the embedded element technique is used to specify a group of T2D2 elements that lie embedded in a group of CPE4R elements whose response will be used to constrain the translational degrees of freedom of the embedded nodes. At concrete/CFRP interface, two dimensional cohesive elements, i.e. COH2D4, were used to model the very thin layer of adhesive. Finally, two dimensional beam elements, B21, were used to model CFRP strip. Only half of the beam was modeled by taking advantage of symmetry. The number of nodes and elements are summarized in Table 6.

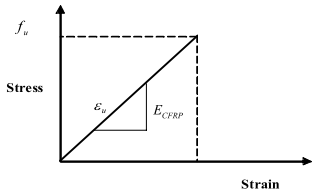

Figure 7. Stress-strain relationship of CFRP.

Table 6. Number of nodes and elements used in mesh sensitivity studies

Test Beams	Coarse mesh		Fine mesh	
	No. of Nodes	No. of Elements	No. of Nodes	No. of Elements
RH-B5	1329	1138	4093	3726
FK-B5	1674	1450	5231	4798

RESULTS AND DISCUSSION

Verification of the proposed material constitutive models First of all, the validity of the material models for concrete and steel is examined by comparing the numerical results of control beams with the experimental data (Fanning & Kelly, 2001; Rahimi & Hutchinson, 2001). Figures 9 and 10 show load-deflection curves of control beams failing by concrete crushing and the comparison of cracks pattern obtained from FE analysis and experimental data, respectively. It can be seen that the analysis results agree well with the experimental data with error within 10% of the peak load. In addition, crack patterns obtained from FE analysis also show good agreement with the experimental data. The contour plot of tensile strain within concrete shows the areas of exceeding tensile strains (>0.0015), indicating by green and red colors. These areas, therefore, are the location of cracks developed in concrete. Hence, these results indicate that the material models chosen for FE analysis are proved to be able to simulate the behavior of reinforced concrete beam and will be further used in the subsequent analysis.

Non-linear analysis of RC beams strengthened with CFRP

The results of the FE study are presented and discussed in this section. First of all, a comparison of load-deflection response at mid span of RC beams strengthened with CFRP between FE analysis and experimental data is undertaken as shown in Figure 11. Overall, the predictions of FE analysis agree closely with the experimental data. All test beams except beam FK-B3 fail by cover failure. For the case of beam FK-B3 (strengthened by CFRP along its full length), it fails by shear failure. This is due to the sufficient anchorage at the supports in which preventing the beam from cover failure.

After validating FE models with experimental data, various parameters have been investigated including loading capacity, failure pattern, shear stresses distribution between concrete/CFRP interface and strains distribution in tensile steel rebar and CFRP plates. The results of each parametric study can be summarized as follows;

Loading capacity

Load-deflection response at mid span for RC beams strengthened with CFRP are plotted and compared with the experimental data as shown in Figures 12a-12c. It can be seen that strengthened RC beams with CFRP increase flexural capacity of the beams by approximately 70% of its original capacity. For the case of Rahimi's experiment, the flexural performance can be enhanced

even with a relatively small thickness of CFRP added to the beam (RH-B3). For the case of high percentage of conventional reinforcement (RH-C3), only slightly increase of loading capacity can be obtained. This is due to the effect of over reinforcement at the tension side of the beams which leads to failure of concrete at the compression zone, i.e. concrete crushing. These failure modes lead to premature failure of the beam occurring before the ultimate flexural capacity. By increasing the thickness of CFRP (RH-B5 and RH-C5), the beams are stiffer and stronger which causes the reduction of mid span deflections. For the case of Fanning's experiment, they investigated the effect of plate length on the loading capacity of the RC beams. The test beams have rather high percentage of conventional reinforcement. Figure 11c shows loading capacity of test beams with varying plate lengths. Loading capacity increases by approximately 50% of its original capacity while the deflection capacity reduces by the same amount for all test beams. This indicates that plate length has a little effect on loading capacity of the beams as long as the strengthened length is greater than 50% of shear span. These results clearly show that the loading capacity of the plated beams is influenced not only the original stiffness of the beams but also the type and amount of external reinforcement.

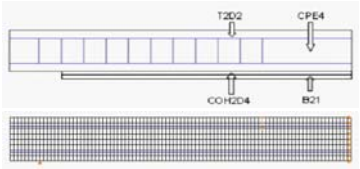

Figure 8. Finite element model of test beams.

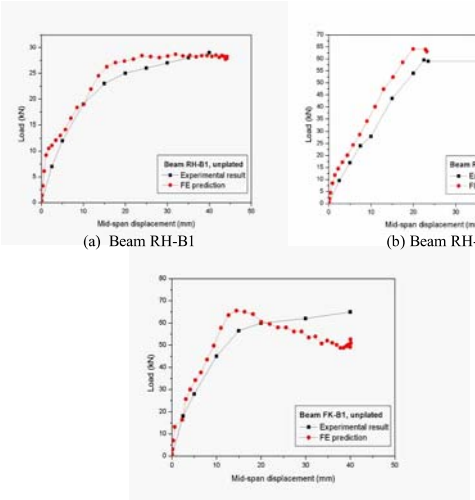

(a) Beam RH-B1 (b) Beam RH-C1

(c) Beam FK-B1

Figure 9. Load-deflection of control beam failing by concrete crushing.

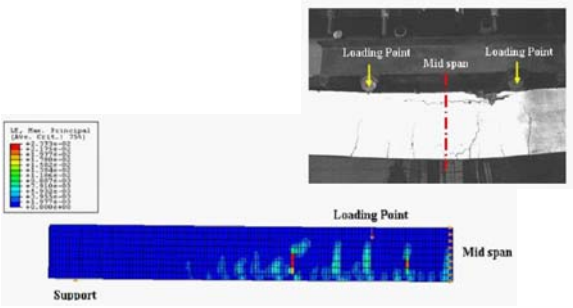

Figure 10. Comparison of cracks pattern obtained from FE analysis and experimental data.

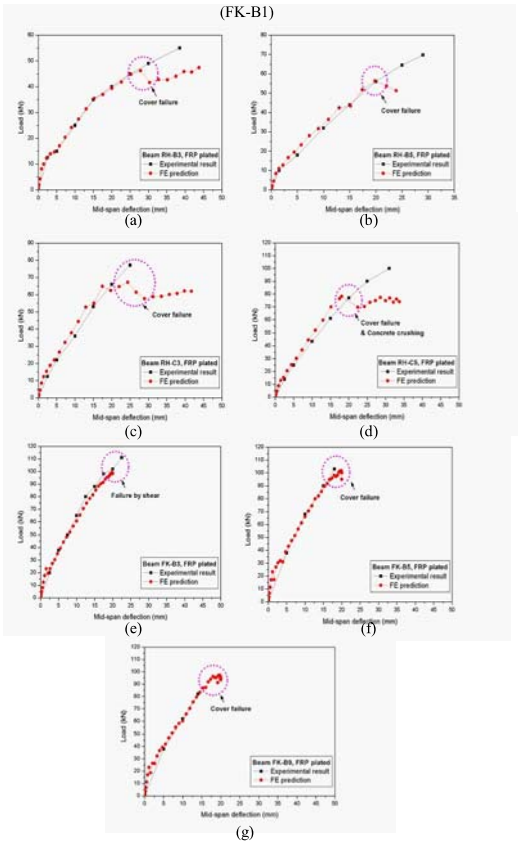

Figure 11. Comparison of load-deflection response at mid span of RC beams strengthened with CFRP between FE analysis and experimental data.

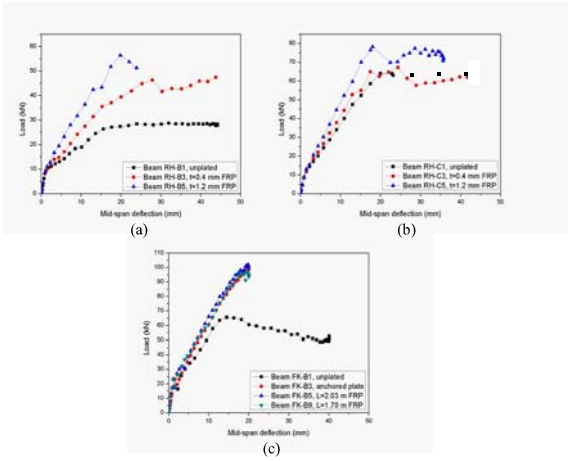

Figure 12. Parametric studies of RC beams strengthened with CFRP.

Shear stresses between concrete/CFRP interface

The insertion of cohesive elements between concrete/CFRP interface has a significant effect on the determination of the shear stresses at the concrete/CFRP interface. This is shown in Figures 13 and 14, in which the shear stresses can be captured and compared with the experimental data. The stress distribution presents many discontinuities along the plate. However the trend of the distribution can be obtained as indicated by the trend line. From Figure 13, the peak stresses occur at the plate ends and starts to decay as the distance from the plate ends is increased. It is evident that the progressive de-cohesion of the laminate from the concrete face initiating in the area nesr to the point of high shear stress and leading to almost complete delamination and then to failure. By increasing the thickness of CFRP plates, the shear stresses concentration at the plate ends increase. For the case of Fanning's experiment (see Figure 14), shear stresses of the beam FK-B3 are rather small and show no stress concentration at the plate ends. This is due to the effect of anchorage at the supports of the beam. The beam is then failed by shear failure in the shear span of the beam instead of concrete cover failure. For the case of the beam FK-B5, the same evident as for the case of Rahimi's experiment is obtained. By reducing the CFRP length, the shear stresses concentration at the plate ends increase. This can be

concluded that the premature failure of the strengthened beams originate from the flexure-shear crack closest to the plate ends and progress towards the tension steel, until ripping of the concrete cover take place as shown in the contour plots in Figures 13 and 14.

Strains distribution in CFRP plates

Figures 15a-15e show strain distributions obtained from both experiment and FE analysis. Increasing in CFRP plate thicknessleads to the reduction of strain in CFRP plates. These results confirm that increasing in the thickness of CFRP plates leads to stiffer and stronger beam which therefore resulting in the reduction of mid span deflections. Figures 15c and 15d compare the strain distributions between experimental and FE analysis in which good agreement is obtained.

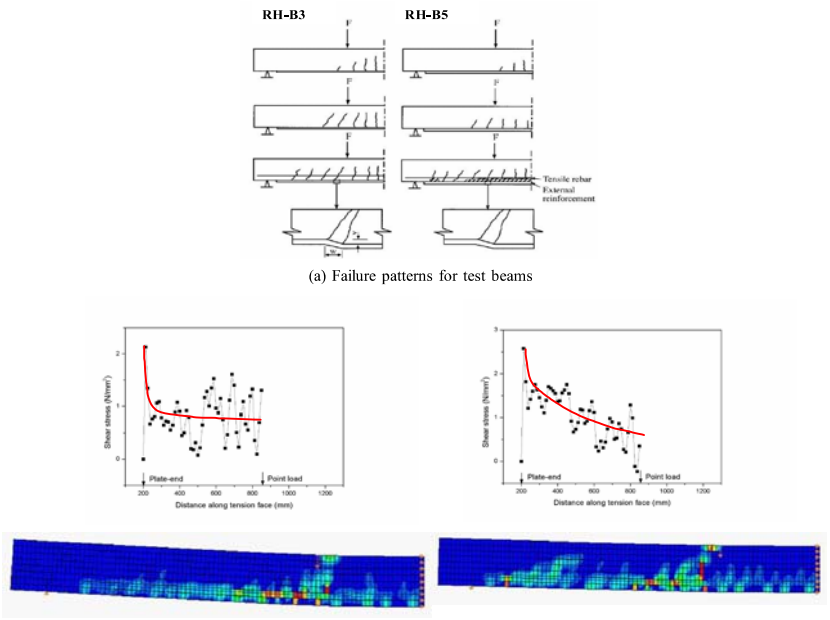

(a) Failure patterns for test beams

(b) Finite element prediction

Figure 13. Comparisons of failure patterns for Rahimi's experiment.

(a) Failure patterns for test beams

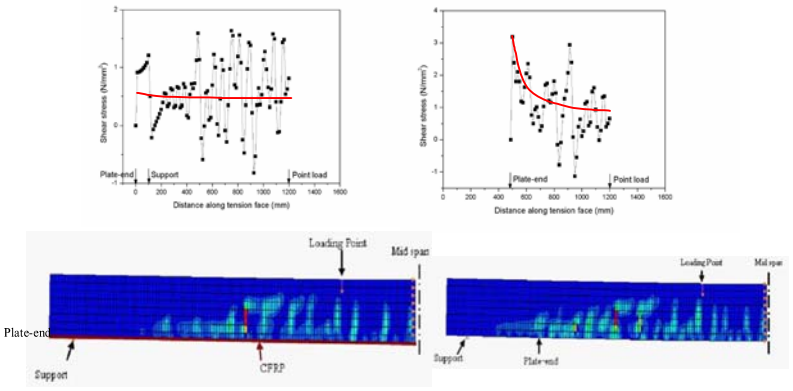

(b) Finite element prediction

Figure 14. Comparison of failure patterns for Fanning's experiment

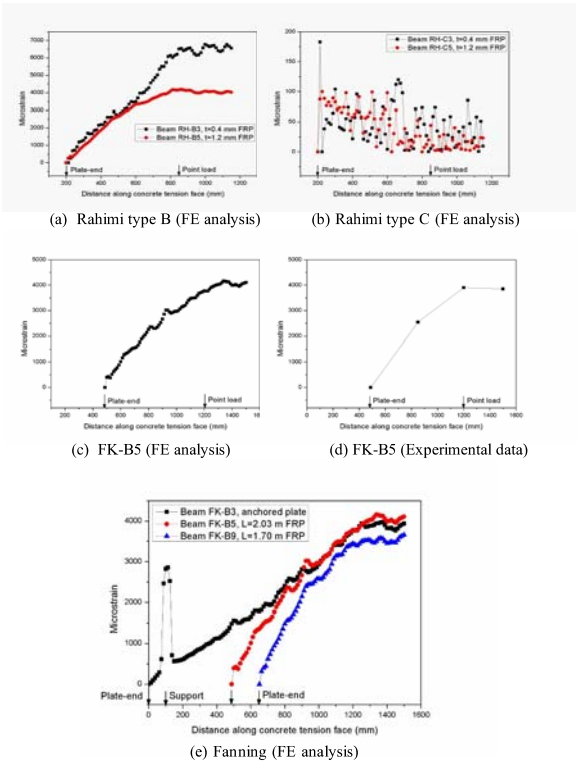

(a) Rahimi type B (FE analysis) (b) Rahimi type C (FE analysis)

(c) FK-B5 (FE analysis) (d) FK-B5 (Experimental data)

(e) Fanning (FE analysis)

Figure 15. Schematic strains distribution in CFRP plates

Effect of mesh sensitivity on failure assessment of RC beams strengthened with CFRP plates

In order to investigate the cause of discontinuities of shear stresses distribution at the concrete/CFRP interface, mesh refinement of FE models (for case RH-B5 and FK-B5) have been carried out as summarized in Table 6. After performing FE analysis, the shear stresses distribution of both test beams are plotted as presented in Figures 16 and 17 for Rahimi's experiment and Fanning's experiment, respectively. It is observed that the results of both meshes show similar trend and the discontinuities of strains distribution are still appearing. Nevertheless, the models with finer mesh present a clear location of cracks as shown in contour plot (see Figures 16b and 17b). When comparing the shear stresses distribution with contour plot of cracks locations, it is observed that the discontinuities of the curves are actually associated with the location of cracks occurring at concrete beams. It can be seen that crack patterns obtained from FE analysis show good agreement with experimental data. As mentioned in previous section, there were a number of close-form solutions for determine the shear stresses distribution. Therefore, the results from FE analysis are then compared with one of the most widely used close-form solutions proposed by Smith and Teng (Smith & Teng, 2001). It is found that the close-form solution overestimates the shear stresses at the cut-off point and decay sharply. When increasing distance from CFRP cut-off point to shear span, the close-form solution appears to underestimate prediction. At the moment span, both predictions show almost the same value of shear stresses. The results from this study confirm that the progressive de-cohesion of the laminate from the concrete face initiating in the area near to the point of high shear stresses and leading to almost complete delamination and then to failure.

CONCLUSIONS

The finite element study of RC beams strengthened with CFRP plates has been performed. Cohesive elements were used to model concrete/CFRP interface in order to capture the interaction between CFRP and concrete beams. First of all, FE models of RC control beams and RC beams strengthened with CFRP plates were analyzed and compared with experimental data. It has been demonstrated that sufficient accuracy of load-displacement prediction can be obtained from FE models. After that parametric studies including effect of CFRP thickness, CFRP length, types of conventional reinforcement were investigated and illustrated in terms of loading capacity, failure pattern and strain distribution in CFRP plates. Again, good agreement was obtained for all cases. By taking advantage of the ability of cohesive element on modeling adhesives and bonded interfaces, shear stresses distribution between concrete/CFRP interface were obtained. It was observed that the discontinuities of the curves are actually associated with the location of cracks occurring at concrete beams. Furthermore, shear stresses distribution obtained from FE analysis were compared with one of the most widely used close-form solutions proposed by Smith and Teng

(Smith & Teng, 2001). It was foundthat both results give a similar trend. Nevertheless, due to specific assumptions and limitations during derivation of close-form solution, the predictions gave uniform distribution and slightly underestimated shear stresses distribution. Therefore, it can be concluded that FE model of the beams in which concrete/CFRP interface is modeled using cohesive elements can be used to assess the failure of RC beams strengthened with CFRP plates and also foretell its failure pattern.

Table 6. Number of nodes and elements used in mesh sensitivity studies

Test Beams	Coarse mesh		Fine mesh	
	No. of Nodes	No. of Elements	No. of Nodes	No. of Elements
RH-B5	1329	1138	4093	3726
FK-B5	1674	1450	5231	4798

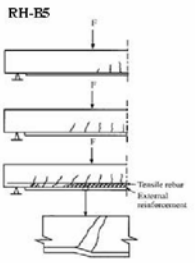

(a) Failure sketch from Rahimi's experiment (beam RH-B5)

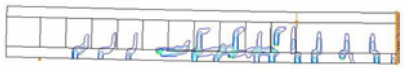

(b) Cracks pattern from FE analysis

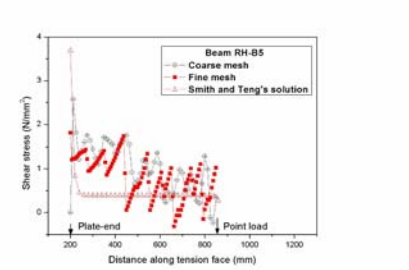

Figure 16. Failure assessment of Rahimi's experiment.

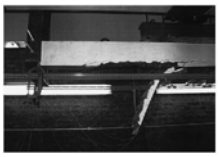

(a) Failure photo from Fanning's experiment (beam FK-B5)

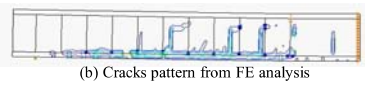

(b) Cracks pattern from FE analysis

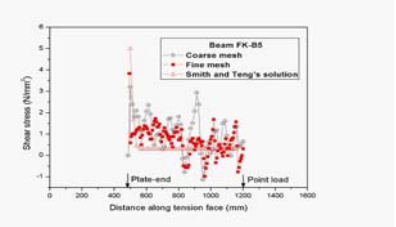

(c) Shear stresses at concrete/CFRP interface

Figure 17. Failure assessment of Fanning's experiment.

ACKNOWLEDGEMENT

This project was supported by Ubonratchathani University, Thailand. The support is gratefully acknowledged.

REFERENCES

Arduini, M., & Nanni, A. (1997). Behavior of pre-cracked RC beams strengthened with carbon FRP sheets. *ASCE Journal of Composites for Construction, 1*, 63-70.

Arduini, M., Tommaso, A. D., & Nanni, A.(1997). Brittle failure in FRP plate and sheet bonded beams. *ACI structural Journal, 94*, 363-370.

Bazant, Z. (1986). Mechanics of distributed cracking. *Appl Mech Rev, 39*, 675-705.

Bonacci, J. F., & Maleej, M. (2000). Externally bonded fiber-reinforced polymer for rehabilitation of corrosion damaged concrete beams. *ACI Structural Journal, 97*, 703-711.

Fanning, P., & Kelly, O. (2001). Ultimate response of RC beams strengthened with CFRP plates. *ASCE Journal of Composites for Construction, 5*, 122-127.

Grace, N. F., Soliman, A. K., Abdel-Sayed, G., & Saleh, K. R. (1998). Behavior and ductility of simple and continuous FRP reinforced beams. *ASCE Journal of Composites for Construction, 2*, 186-194.

Heffernan, P. J., & Erki, M. A. (1996). Equivalent capacity and efficiency of reinforced concrete beams strengthened with carbon fiber reinforced plastic sheets. *Canadian Journal of Civil Engineering, 23*, 21-29.

Hibbitt, Karlson., & Sorensen. (2005). *ABAQUS/Explicit User's Manual*, Version 6.5. Inc. Pawtucket, RI.

Hormann, M., Seible, F., Seim, W., & Karbhari, V. (2001). External FRP post-strengthening of scaled concrete slabs. *ASCE Journal of Composites for Construction, 5*, 67-75.

Lubliner, J., Oliver, J., Oller, S., & Onate, E. (1989). Plastic-damage model for concrete. *Int J Solids Struct, 25*, 299-326.

Malek, A. M., Saadatmanesh, H., & Ehsani, M. R. (1998). Prediction of failure load of RC beams strengthened with FRP plate due to stress concentration at the plate ends. *ACI Structural Journal, 95*, 142-152.

Mayo, R., Nanni, A., Watkins, S., & Barker, M. (2000). *Strengthening of bridge G-270 with externally bonded CFRP sheets.* USA: Technical Report R198-102, Missouri Department of Transportation.

Nguyen, D. M., Chan, T. K., & Cheong, H. K. (2001). Brittle Failure and Bond development length of CFRP Concrete Beams. *ASCE Journal of Composites for Construction, 5*, 12-17.

PDA Engineering. (1993). *Patran V 9.0 User Manual*, USA.

Rahimi, H., & Hutchinson, A. (2001). Concrete beams strengthened with externally bonded FRP plates. *ASCE Journal of Composites for Construction, 5*, 44-56.

Ritchie, P. A., Thomas, D. A., Lu, L. W., & Comely, G. M. (1991). External reinforcement of concrete beams using fiber reinforced plastics. *ACI Structural Journal, 67*, 490-500.

Robert, T. M. (1989). Approximate analysis of shear and normal stress concentrations in the adhesive layer of plated RC beams. *ASCE Journal of Structural Engineering, 67*, 229-233.

Ross, C. M., Jerome, D. M., Tedesco, J. W., & Hughes, M. L. (1999). Strengthening of reinforced concrete beams with externally bonded composite laminates. *ACI Structural Journal, 96*, 212-220.

Saadatmanesh, H., & Ehsani, M. R. (1991). RC beams strengthened with GFRP plates I: Experimental study. *ASCE Journal of Structural Engineering, 117*, 3417-3433.

Sebastian, W. (2001). Significance of midspan debonding failure in FRP-plated concrete beams. *ASCE Journal of Structural Engineering, 127*, 792-798.

Shahawy, M. A., Arockiasamy, M., Beitelman, T., & Sowrirajan, R. (1996). Reinforced concrete rectangular beams strengthened with CFRP laminates. *Composites: Part B, 27*, 225-233.

Sharif, A., Al-Sulaimani, G. J., Basunbul, I. A., Baluch, M. H., & Ghaleb, B. N. (1994). Strengthening of initially loaded reinforced concrete beams using FRP plates. *ACI Structural Journal, 91*, 160-168.

Smith, S. T., & Teng, J. G. (2001). *Shear Stresses in Plated Beams. Eng. Struct, 23*, 857-871.

Takeda, K., Mitsui, Y., Murakami, K., Sakai, H., & Nakamura, M. (1996). Flexural behavior of reinforced concrete beams strengthened with carbon fiber sheets. *Composites: Part A, 27*, 981-987.

Triantafillou, T. C., & Plevris, N. (1992). Strengthening of RC beams with epoxy-bonded fiber composite materials. *Materials and Structures, 25*, 201-211.

Wong, R. S. Y., Vecchio, F. J., & Nanni, A. (2003). Towards modeling of reinforced concrete members with externally-bonded beams. *ACI structural Journal, 100*, 47-55.

Ziraba, Y. N., & Baluch, M. H. (1995). Computational model for reinforced concrete beams strengthened by epoxy bonded steel plates. Finite Elem Anal Des, 20, 253-271.